# Implications of the KamLAND measurement on the lepton flavor mixing matrix and the neutrino mass matrix

Wan-lei Guo* and Zhi-zhong Xing†

*CCAST (World Laboratory), P.O. Box 8730, Beijing 100039, China*

*and Institute of High Energy Physics, Chinese Academy of Sciences, P.O. Box 918 (4), Beijing 100039, China‡*

We explore some important implications of the KamLAND measurment on the lepton flavor mixing matrix $V$ and the neutrino mass matrix $M$. The model-independent constraints on nine matrix elements of $V$ are obtained to a reasonable degree of accuracy. We find that nine two-zero textures of $M$ are compatible with current experimental data, but two of them are only marginally allowed. Instructive predictions are given for the absolute neutrino masses, Majorana phases of $CP$ violation, effective masses of the tritium beta decay, and neutrinoless double beta decay.

## I. INTRODUCTION

The KamLAND experiment [1] is attempting to confirm the large-mixing-angle (LMA) Mikheyev-Smirnov-Wolfenstein (MSW) solution [2] to the long-standing solar neutrino problem. In addition, the K2K long-baseline experiment [3] has unambiguously observed a reduction of $\nu_\mu$ flux and a distortion of the energy spectrum. These new measurements, together with the compelling SNO evidence [4] for the flavor conversion of solar $\nu_e$ neutrinos and the Super-Kamiokande evidence [5] for the deficit of atmospheric $\nu_\mu$ neutrinos, convince us that the hypothesis of neutrino oscillations is actually correct. We are then led to the conclusion that neutrinos are massive and lepton flavors are mixed.

The mixing of lepton flavors means that there is a mismatch between neutrino mass eigenstates ($\nu_1, \nu_2, \nu_3$) and neutrino flavor eigenstates ($\nu_e, \nu_\mu, \nu_\tau$) in the basis where the charged lepton mass matrix is diagonal:

$$\begin{pmatrix} \nu_e \\ \nu_\mu \\ \nu_\tau \end{pmatrix} = \begin{pmatrix} V_{e1} & V_{e2} & V_{e3} \\ V_{\mu1} & V_{\mu2} & V_{\mu3} \\ V_{\tau1} & V_{\tau2} & V_{\tau3} \end{pmatrix} \begin{pmatrix} \nu_1 \\ \nu_2 \\ \nu_3 \end{pmatrix}. \quad (1)$$

The matrix elements $|V_{e1}|$, $|V_{e2}|$, $|V_{e3}|$, and $|V_{\mu3}|$ can simply be related to the mixing factors of solar [1,4], atmospheric [5], and CHOOZ reactor [6] neutrino oscillations in the following way:

$$\sin^2 2\theta_{\text{sun}} = 4|V_{e1}|^2 |V_{e2}|^2,$$

$$\sin^2 2\theta_{\text{atm}} = 4|V_{\mu3}|^2 (1 - |V_{\mu3}|^2),$$

$$\sin^2 2\theta_{\text{chz}} = 4|V_{e3}|^2 (1 - |V_{e3}|^2). \quad (2)$$

Taking account of the unitarity of $V$, one may reversely express $|V_{e1}|$, $|V_{e2}|$, $|V_{e3}|$, $|V_{\mu3}|$, and $|V_{\tau3}|$ in terms of $\theta_{\text{sun}}$, $\theta_{\text{atm}}$, and $\theta_{\text{chz}}$ [7]:

*Email address: guowl@mail.ihep.ac.cn

†Email address: xingzz@mail.ihep.ac.cn

‡Mailing address.

$$|V_{e1}| = \frac{1}{\sqrt{2}} \sqrt{\cos^2\theta_{\text{chz}} + \sqrt{\cos^4\theta_{\text{chz}} - \sin^2 2\theta_{\text{sun}}}},$$

$$|V_{e2}| = \frac{1}{\sqrt{2}} \sqrt{\cos^2\theta_{\text{chz}} - \sqrt{\cos^4\theta_{\text{chz}} - \sin^2 2\theta_{\text{sun}}}},$$

$$|V_{e3}| = \sin\theta_{\text{chz}},$$

$$|V_{\mu3}| = \sin\theta_{\text{atm}},$$

$$|V_{\tau3}| = \sqrt{\cos^2\theta_{\text{chz}} - \sin^2\theta_{\text{atm}}}. \quad (3)$$

Current experimental information on $\theta_{\text{sun}}$, $\theta_{\text{atm}}$, and $\theta_{\text{chz}}$ allows us to get very instructive constraints on the lepton flavor mixing matrix $V$. One purpose of this paper is therefore to examine how accurately we can recast $V$ from the present KamLAND, K2K, SNO, Super-Kamiokande, and CHOOZ measurements.

Another purpose of this paper is to confront two-zero textures of the neutrino mass matrix with the new KamLAND data, so as to single out the most favorable texture(s) in phenomenology. In the flavor basis chosen above, the Majorana neutrino mass matrix can be written as

$$M = V \begin{pmatrix} m_1 & 0 & 0 \\ 0 & m_2 & 0 \\ 0 & 0 & m_3 \end{pmatrix} V^{\text{T}}, \quad (4)$$

where $m_i$ (for $i=1,2,3$) are physical masses of three neutrinos. In the assumption of the LMA solution for solar neutrino oscillations, a classification of $M$ with two vanishing entries has been done in an analytically approximate way [8,9]. Our present analysis is different from the previous ones in two important aspects: (1) we carry out a careful numerical analysis of every two-zero pattern of the neutrino mass matrix $M$ to pin down its complete parameter space; (2) we present the quantitative predictions for allowed ranges of the absolute neutrino masses, the Majorana phases of $CP$ violation, and the effective masses of the tritium beta decay ($\langle m \rangle_e$) and neutrinoless double beta decay ($\langle m \rangle_{ee}$).

**67** 053002-1

The remaining part of this paper is organized as follows. With the help of current data, we derive the model-independent constraints on nine elements of the lepton flavor mixing matrix in Sec. II. Section III is devoted to a detailed analysis of the parameter space for every two-zero texture of the neutrino mass matrix. We obtain instructive predictions for the neutrino mass spectrum and Majorana phases of $CP$ violation as well as $\langle m \rangle_e$ and $\langle m \rangle_{ee}$ in Sec. IV. Finally, a brief summary is given in Sec. V.

## II. CONSTRAINTS ON THE LEPTON FLAVOR MIXING MATRIX

As already shown in Eq. (3), five matrix elements of $V$ can be determined or constrained from current experimental data. The other four matrix elements ($|V_{\mu 1}|$, $|V_{\mu 2}|$, $|V_{\tau 1}|$, and $|V_{\tau 2}|$) are entirely unrestricted, however, unless one of them or the rephasing invariant of $CP$ violation of $V$ (defined as $J$ [10]) is measured. A realistic way to get rough but useful constraints on those four unknown elements is to allow the Dirac phase of $CP$ violation in $V$ to vary between 0 and $\pi$ [11], such that one can find out the maximal and minimal magnitudes of each matrix element. To see this point more clearly, we adopt the standard parametrization $V = UP$ [12], where

$$U = \begin{pmatrix} c_x c_z & s_x c_z & s_z \\ -c_x s_y s_z - s_x c_y e^{-i\delta} & -s_x s_y s_z + c_x c_y e^{-i\delta} & s_y c_z \\ -c_x c_y s_z + s_x s_y e^{-i\delta} & -s_x c_y s_z - c_x s_y e^{-i\delta} & c_y c_z \end{pmatrix} \tag{5}$$

with $s_x \equiv \sin\theta_x$, $c_x \equiv \cos\theta_x$, and so on; and

$$P = \begin{pmatrix} e^{i\rho} & 0 & 0 \\ 0 & e^{i\sigma} & 0 \\ 0 & 0 & 1 \end{pmatrix}. \tag{6}$$

The advantage of this representation is that the neutrinoless double beta decay is associated with the Majorana phases $\rho$ and $\sigma$, while $CP$ violation in normal neutrino oscillations depends separately on the Dirac phase $\delta$. Note that three mixing angles ($\theta_x, \theta_y, \theta_z$), which are all arranged to lie in the first quadrant, can be written as

$$\tan\theta_x = \frac{|V_{e2}|}{|V_{e1}|},$$

$$\tan\theta_y = \frac{|V_{\mu 3}|}{|V_{\tau 3}|},$$

$$\sin\theta_z = |V_{e3}|. \tag{7}$$

It is then straightforward to obtain

$$|V_{\mu 1}| = \frac{\left| |V_{e2}||V_{\tau 3}| + |V_{e1}||V_{e3}||V_{\mu 3}| \, e^{i\delta} \right|}{1 - |V_{e3}|^2},$$

$$|V_{\mu 2}| = \frac{\left| |V_{e1}||V_{\tau 3}| - |V_{e2}||V_{e3}||V_{\mu 3}| \, e^{i\delta} \right|}{1 - |V_{e3}|^2},$$

$$|V_{\tau 1}| = \frac{\left| |V_{e2}||V_{\mu 3}| - |V_{e1}||V_{e3}||V_{\tau 3}| \, e^{i\delta} \right|}{1 - |V_{e3}|^2},$$

$$|V_{\tau 2}| = \frac{\left| |V_{e1}||V_{\mu 3}| + |V_{e2}||V_{e3}||V_{\tau 3}| \, e^{i\delta} \right|}{1 - |V_{e3}|^2}. \tag{8}$$

Varying the Dirac phase $\delta$ from 0 to $\pi$, we are led to the *most generous* ranges of $|V_{\mu 1}|$, $|V_{\mu 2}|$, $|V_{\tau 1}|$, and $|V_{\tau 2}|$:

$$\frac{|V_{e2}||V_{\tau 3}| - |V_{e1}||V_{e3}||V_{\mu 3}|}{1 - |V_{e3}|^2} \leq |V_{\mu 1}|$$

$$\leq \frac{|V_{e2}||V_{\tau 3}| + |V_{e1}||V_{e3}||V_{\mu 3}|}{1 - |V_{e3}|^2},$$

$$\frac{|V_{e1}||V_{\tau 3}| - |V_{e2}||V_{e3}||V_{\mu 3}|}{1 - |V_{e3}|^2} \leq |V_{\mu 2}|$$

$$\leq \frac{|V_{e1}||V_{\tau 3}| + |V_{e2}||V_{e3}||V_{\mu 3}|}{1 - |V_{e3}|^2},$$

$$\frac{|V_{e2}||V_{\mu 3}| - |V_{e1}||V_{e3}||V_{\tau 3}|}{1 - |V_{e3}|^2} \leq |V_{\tau 1}|$$

$$\leq \frac{|V_{e2}||V_{\mu 3}| + |V_{e1}||V_{e3}||V_{\tau 3}|}{1 - |V_{e3}|^2},$$

$$\frac{|V_{e1}||V_{\mu 3}| - |V_{e2}||V_{e3}||V_{\tau 3}|}{1 - |V_{e3}|^2} \leq |V_{\tau 2}|$$

$$\leq \frac{|V_{e1}||V_{\mu 3}| + |V_{e2}||V_{e3}||V_{\tau 3}|}{1 - |V_{e3}|^2}. \tag{9}$$

Note that the lower and upper bounds of each matrix element turn to coincide with each other in the limit $|V_{e3}| \to 0$. Because of the smallness of $|V_{e3}|$, the ranges obtained in Eq. (9) should be quite restrictive. Hence it makes sense to recast the lepton flavor mixing matrix even in the absence of any experimental information on $CP$ violation.

In view of the present experimental data from KamLAND [1], K2K [3], SNO [4], Super-Kamiokande [5], and CHOOZ [6], we have $0.25 \leq \sin^2\theta_{\text{sun}} \leq 0.40$ [13], $0.92 < \sin^2 2\theta_{\text{atm}} \leq 1.0$, and $0 \leq \sin^2 2\theta_{\text{chz}} < 0.1$ at the 90% confidence level. Namely,

$$30.0° \leq \theta_{\text{sun}} \leq 39.2°,$$

$$36.8° < \theta_{\text{atm}} < 53.2°,$$

$$0° \leq \theta_{\text{chz}} < 9.2°. \tag{10}$$

Using these inputs, we calculate the numerical ranges of $|V_{e1}|$, $|V_{e2}|$, $|V_{e3}|$, $|V_{\mu3}|$, and $|V_{\tau3}|$ from Eq. (3). Then the allowed ranges of $|V_{\mu1}|$, $|V_{\mu2}|$, $|V_{\tau1}|$, and $|V_{\tau2}|$ can be found with the help of Eq. (9). Our numerical results are summarized as

$$|V| = \begin{pmatrix} 0.70-0.87 & 0.50-0.69 & <0.16 \\ 0.20-0.61 & 0.34-0.73 & 0.60-0.80 \\ 0.21-0.63 & 0.36-0.74 & 0.58-0.80 \end{pmatrix}. \quad (11)$$

This result is certainly more restrictive than that obtained in Ref. [11] before the KamLAND measurement.

Note that the rephasing invariant of *CP* violation reads as follows:

$$\begin{aligned} J &= \frac{|V_{e1}||V_{e2}||V_{e3}||V_{\mu3}||V_{\tau3}|}{1-|V_{e3}|^2}\sin\delta \\ &= \frac{\sqrt{\sin^2 2\theta_{\text{sun}}(\sin^2 2\theta_{\text{atm}}+4\sin^2\theta_{\text{atm}}\sin^2\theta_{\text{chz}})}}{4\cos^2\theta_{\text{chz}}}\sin\theta_{\text{chz}}\sin\delta. \end{aligned}$$
$$(12)$$

The terms proportional to $4\sin^2\theta_{\text{atm}}\sin^2\theta_{\text{chz}}$ in $J$, which may correct the leading term up to 5% (for $\theta_{\text{atm}}=45°$ and $\theta_{\text{chz}}=9°$), were not taken into account in Ref. [11]. By use of Eq. (10), we find $J \leqslant 0.039\sin\delta$. This result implies that the magnitude of $J$ can maximally be 0.039, leading probably to observable *CP*-violating effects in long-baseline neutrino oscillations.

## III. TWO-ZERO TEXTURES OF THE NEUTRINO MASS MATRIX

The symmetric neutrino mass matrix $M$ totally has six independent complex entries. If two of them vanish, i.e., $M_{ab}=M_{pq}=0$, we obtain two constraint equations:

$$m_1 U_{a1}U_{b1}e^{2i\rho}+m_2 U_{a2}U_{b2}e^{2i\sigma}+m_3 U_{a3}U_{b3}=0,$$
$$m_1 U_{p1}U_{q1}e^{2i\rho}+m_2 U_{p2}U_{q2}e^{2i\sigma}+m_3 U_{p3}U_{q3}=0,$$
$$(13)$$

where $a$, $b$, $p$, and $q$ run over $e$, $\mu$, and $\tau$, but $(p,q) \neq (a,b)$. Solving Eq. (12), we arrive at [9]

$$\frac{m_1}{m_3}e^{2i\rho}=\frac{U_{a3}U_{b3}U_{p2}U_{q2}-U_{a2}U_{b2}U_{p3}U_{q3}}{U_{a2}U_{b2}U_{p1}U_{q1}-U_{a1}U_{b1}U_{p2}U_{q2}},$$

$$\frac{m_2}{m_3}e^{2i\sigma}=\frac{U_{a1}U_{b1}U_{p3}U_{q3}-U_{a3}U_{b3}U_{p1}U_{q1}}{U_{a2}U_{b2}U_{p1}U_{q1}-U_{a1}U_{b1}U_{p2}U_{q2}}.$$
$$(14)$$

This result implies that two neutrino mass ratios $(m_1/m_3, m_2/m_3)$ and two Majorana-type *CP*-violating phases $(\rho,\sigma)$ can fully be determined in terms of three mixing angles $(\theta_x,\theta_y,\theta_z)$ and the Dirac-type *CP*-violating phase $(\delta)$. Thus one may examine whether a two-zero texture of $M$ is empirically acceptable or not by comparing its prediction for the ratio of two neutrino mass-squared differ-

ences with the result extracted from current experimental data on solar and atmospheric neutrino oscillations:

$$R_\nu \equiv \frac{|m_2^2-m_1^2|}{|m_3^2-m_2^2|} \approx \frac{\Delta m_{\text{sun}}^2}{\Delta m_{\text{atm}}^2}. \quad (15)$$

Considering the LMA MSW solution confirmed by the KamLAND measurement, we have $5.9\times10^{-5}$ eV$^2 \leqslant \Delta m_{\text{sun}}^2 \leqslant 8.8\times10^{-5}$ eV$^2$ [13,14] at the 90% confidence level. In addition, we have $1.6\times10^{-3}$ eV$^2 \leqslant \Delta m_{\text{atm}}^2 \leqslant 3.9\times10^{-3}$ eV$^2$ [15] at the 90% confidence level. Thus we arrive at $1.5\times10^{-2} \leqslant R_\nu \leqslant 5.5\times10^{-2}$. The allowed ranges of three mixing angles $\theta_x \approx \theta_{\text{sun}}$, $\theta_y \approx \theta_{\text{atm}}$, and $\theta_z \approx \theta_{\text{chz}}$ have been given in Eq. (10). There is no experimental constraint on the *CP*-violating phase $\delta$. Hence we simply take $\delta$ from $0°$ to $360°$ in our numerical calculations.

There are totally fifteen distinct topologies for the structure of $M$ with two independent vanishing entries, as shown in Tables I and II. We work out the explicit expressions of $(m_1/m_3)e^{2i\rho}$ and $(m_2/m_3)e^{2i\sigma}$ for each pattern of $M$ by use of Eq. (14), and list the results in the same tables [16]. With the input values of $\theta_x$, $\theta_y$, $\theta_z$, and $\delta$ mentioned above, we calculate the ratio $R_\nu$ and examine whether it is in the range allowed by current data. This criterion has been used in Refs. [8,9] to pick the phenomenologically favored patterns of $M$ in the LMA case.

Nine of the fifteen two-zero textures of $M$ listed in Table I are found to be in accord with the LMA solution as well as the atmospheric neutrino data. They can be classified into four categories: A (with A$_1$ and A$_2$), B (with B$_1$, B$_2$, B$_3$, and B$_4$), C and D (with D$_1$ and D$_2$). The point of this classification is that the textures of $M$ in each category result in similar physical consequences, which are almost indistinguishable in practice. The other six patterns of $M$ (categories E and F) listed in Table II cannot coincide with current experimental data. In particular, the exact neutrino mass degeneracy ($m_1=m_2=m_3$) is predicted from three textures of $M$ belonging to category F.

Now let us focus on patterns A$_1$, B$_1$, C, and D$_1$ as four typical examples for numerical illustration. Our results for $\sin^2 2\theta_{\text{chz}}$ versus $\delta$ and $\theta_y$ versus $\theta_x$ are shown in Figs. 1–4. Some comments are in order.

(1) For pattern A$_1$, arbitrary values of $\delta$ are allowed if $\sin^2 2\theta_{\text{chz}}$ is large enough ($\geqslant 0.014$). The mixing angles $\theta_x$ and $\theta_y$ may take any values in the ranges allowed by current data. Therefore we conclude that pattern A$_1$ is favored in phenomenology with little fine tuning. A similar conclusion can be drawn for pattern A$_2$.

(2) For pattern B$_1$, $\delta$ is essentially unconstrained if $\sin^2 2\theta_{\text{chz}}$ is extremely close to zero; and only $\delta$ around $90°$ or $270°$ is acceptable if $\sin^2 2\theta_{\text{chz}}$ deviates somehow from zero. Except $\theta_y \neq 45°$, there is no further constraint on the parameter space of $(\theta_x,\theta_y)$. We conclude that pattern B$_1$ with maximal *CP* violation (i.e., $\sin\delta \approx \pm1$) is phenomenologically favored. So are patterns B$_2$, B$_3$, and B$_4$.

(3) For pattern C, $\delta=90°$ or $\delta=270°$ is forbidden. Furthermore, $\theta_y=45°$ is forbidden. We see that the allowed pa-

TABLE I. Nine patterns of the neutrino mass matrix $M$ with two independent vanishing entries, which are *compatible* with the LMA solution and other empirical hypotheses. The analytical results for two ratios of three neutrino mass eigenvalues $(m_1/m_3)e^{2i\rho}$ and $(m_2/m_3)e^{2i\sigma}$ are given in terms of four flavor mixing parameters $\theta_x$, $\theta_y$, $\theta_z$, and $\delta$.

| Pattern of $M$ | Results of $(m_1/m_3)e^{2i\rho}$ and $(m_2/m_3)e^{2i\sigma}$ |
| --- | --- |
| $A_1: \begin{pmatrix} 0 & 0 & \times \\ 0 & \times & \times \\ \times & \times & \times \end{pmatrix}$ | $\dfrac{m_1}{m_3}e^{2i\rho} = +\dfrac{s_z}{c_z^2}\left(\dfrac{s_x s_y}{c_x c_y}e^{i\delta} - s_z\right)$ $\dfrac{m_2}{m_3}e^{2i\sigma} = -\dfrac{s_z}{c_z^2}\left(\dfrac{c_x s_y}{s_x c_y}e^{i\delta} + s_z\right)$ |
| $A_2: \begin{pmatrix} 0 & \times & 0 \\ \times & \times & \times \\ 0 & \times & \times \end{pmatrix}$ | $\dfrac{m_1}{m_3}e^{2i\rho} = -\dfrac{s_z}{c_z^2}\left(\dfrac{s_x c_y}{c_x s_y}e^{i\delta} + s_z\right)$ $\dfrac{m_2}{m_3}e^{2i\sigma} = +\dfrac{s_z}{c_z^2}\left(\dfrac{c_x c_y}{s_x s_y}e^{i\delta} - s_z\right)$ |
| $B_1: \begin{pmatrix} \times & \times & 0 \\ \times & 0 & \times \\ 0 & \times & \times \end{pmatrix}$ | $\dfrac{m_1}{m_3}e^{2i\rho} = \dfrac{s_x c_x s_y(2c_y^2 s_z^2 - s_y^2 c_z^2) - c_y s_z(s_x^2 s_y^2 e^{+i\delta} + c_x^2 c_y^2 e^{-i\delta})}{s_x c_x s_y c_y^2 + (s_x^2 - c_x^2)c_y^3 s_z e^{i\delta} + s_x c_x s_y s_z^2(1 + c_y^2)e^{2i\delta}}e^{2i\delta}$ $\dfrac{m_2}{m_3}e^{2i\sigma} = \dfrac{s_x c_x s_y(2c_y^2 s_z^2 - s_y^2 c_z^2) + c_y s_z(c_x^2 s_y^2 e^{+i\delta} + s_x^2 c_y^2 e^{-i\delta})}{s_x c_x s_y c_y^2 + (s_x^2 - c_x^2)c_y^3 s_z e^{i\delta} + s_x c_x s_y s_z^2(1 + c_y^2)e^{2i\delta}}e^{2i\delta}$ |
| $B_2: \begin{pmatrix} \times & 0 & \times \\ 0 & \times & \times \\ \times & \times & 0 \end{pmatrix}$ | $\dfrac{m_1}{m_3}e^{2i\rho} = \dfrac{s_x c_x c_y(2s_y^2 s_z^2 - c_y^2 c_z^2) + s_y s_z(s_x^2 c_y^2 e^{+i\delta} + c_x^2 s_y^2 e^{-i\delta})}{s_x c_x s_y^2 c_y - (s_x^2 - c_x^2)s_y^3 s_z e^{i\delta} + s_x c_x c_y s_z^2(1 + s_y^2)e^{2i\delta}}e^{2i\delta}$ $\dfrac{m_2}{m_3}e^{2i\sigma} = \dfrac{s_x c_x c_y(2s_y^2 s_z^2 - c_y^2 c_z^2) - s_y s_z(c_x^2 c_y^2 e^{+i\delta} + s_x^2 s_y^2 e^{-i\delta})}{s_x c_x s_y^2 c_y - (s_x^2 - c_x^2)s_y^3 s_z e^{i\delta} + s_x c_x c_y s_z^2(1 + s_y^2)e^{2i\delta}}e^{2i\delta}$ |
| $B_3: \begin{pmatrix} \times & 0 & \times \\ 0 & 0 & \times \\ \times & \times & \times \end{pmatrix}$ | $\dfrac{m_1}{m_3}e^{2i\rho} = -\dfrac{s_y}{c_y}\cdot\dfrac{s_x s_y - c_x c_y s_z e^{-i\delta}}{s_x c_y + c_x s_y s_z e^{+i\delta}}e^{2i\delta}$ $\dfrac{m_2}{m_3}e^{2i\sigma} = -\dfrac{s_y}{c_y}\cdot\dfrac{c_x s_y + s_x c_y s_z e^{-i\delta}}{c_x c_y - s_x s_y s_z e^{+i\delta}}e^{2i\delta}$ |
| $B_4: \begin{pmatrix} \times & \times & 0 \\ \times & \times & \times \\ 0 & \times & 0 \end{pmatrix}$ | $\dfrac{m_1}{m_3}e^{2i\rho} = -\dfrac{c_y}{s_y}\cdot\dfrac{s_x c_y + c_x s_y s_z e^{-i\delta}}{s_x s_y - c_x c_y s_z e^{+i\delta}}e^{2i\delta}$ $\dfrac{m_2}{m_3}e^{2i\sigma} = -\dfrac{c_y}{s_y}\cdot\dfrac{c_x c_y - s_x s_y s_z e^{-i\delta}}{c_x s_y + s_x c_y s_z e^{+i\delta}}e^{2i\delta}$ |
| $C: \begin{pmatrix} \times & \times & \times \\ \times & 0 & \times \\ \times & \times & 0 \end{pmatrix}$ | $\dfrac{m_1}{m_3}e^{2i\rho} = -\dfrac{c_x c_z^2}{s_z}\cdot\dfrac{c_x(s_y^2 - c_y^2) + 2s_x s_y c_y s_z e^{i\delta}}{2s_x c_x s_y c_y - (s_x^2 - c_x^2)(s_y^2 - c_y^2)s_z e^{i\delta} + 2s_x c_x s_y c_y s_z^2 e^{2i\delta}}e^{i\delta}$ $\dfrac{m_2}{m_3}e^{2i\sigma} = +\dfrac{s_x c_z^2}{s_z}\cdot\dfrac{s_x(s_y^2 - c_y^2) - 2c_x s_y c_y s_z e^{i\delta}}{2s_x c_x s_y c_y - (s_x^2 - c_x^2)(s_y^2 - c_y^2)s_z e^{i\delta} + 2s_x c_x s_y c_y s_z^2 e^{2i\delta}}e^{i\delta}$ |
| $D_1: \begin{pmatrix} \times & \times & \times \\ \times & 0 & 0 \\ \times & 0 & \times \end{pmatrix}$ | $\dfrac{m_1}{m_3}e^{2i\rho} = -\dfrac{c_z^2}{s_z}\cdot\dfrac{c_x s_y}{s_x c_y + c_x s_y s_z e^{i\delta}}e^{i\delta}$ $\dfrac{m_2}{m_3}e^{2i\sigma} = +\dfrac{c_z^2}{s_z}\cdot\dfrac{s_x s_y}{c_x c_y - s_x s_y s_z e^{i\delta}}e^{i\delta}$ |
| $D_2: \begin{pmatrix} \times & \times & \times \\ \times & \times & 0 \\ \times & 0 & 0 \end{pmatrix}$ | $\dfrac{m_1}{m_3}e^{2i\rho} = +\dfrac{c_z^2}{s_z}\cdot\dfrac{c_x c_y}{s_x s_y - c_x c_y s_z e^{i\delta}}e^{i\delta}$ $\dfrac{m_2}{m_3}e^{2i\sigma} = -\dfrac{c_z^2}{s_z}\cdot\dfrac{s_x c_y}{c_x s_y + s_x c_y s_z e^{i\delta}}e^{i\delta}$ |

TABLE II. Six patterns of the neutrino mass matrix $M$ with two independent vanishing entries, which are *incompatible* with the LMA solution and other empirical hypotheses. The analytical results for two ratios of three neutrino mass eigenvalues $(m_1/m_3)e^{2i\rho}$ and $(m_2/m_3)e^{2i\sigma}$ are given in terms of four flavor mixing parameters $\theta_x$, $\theta_y$, $\theta_z$, and $\delta$.

| Pattern of $M$ | Results of $(m_1/m_3)e^{2i\rho}$ and $(m_2/m_3)e^{2i\sigma}$ |
|---|---|
| $E_1:\begin{pmatrix} \mathbf{0} & \times & \times \\ \times & \mathbf{0} & \times \\ \times & \times & \times \end{pmatrix}$ | $\dfrac{m_1}{m_3}e^{2i\rho}=-\dfrac{1}{c_yc_z^2}\cdot\dfrac{s_x^2s_y^2(c_z^2-s_z^2)-c_xc_ys_z^2(c_xc_y-2s_xs_ys_ze^{i\delta})e^{-2i\delta}}{(s_x^2-c_x^2)c_y+2s_xc_xs_ys_ze^{i\delta}}e^{2i\delta}$ <br><br> $\dfrac{m_2}{m_3}e^{2i\sigma}=+\dfrac{1}{c_yc_z^2}\cdot\dfrac{c_x^2s_y^2(c_z^2-s_z^2)-s_xc_ys_z^2(s_xc_y+2c_xs_ys_ze^{i\delta})e^{-2i\delta}}{(s_x^2-c_x^2)c_y+2s_xc_xs_ys_ze^{i\delta}}e^{2i\delta}$ |
| $E_2:\begin{pmatrix} \mathbf{0} & \times & \times \\ \times & \times & \times \\ \times & \times & \mathbf{0} \end{pmatrix}$ | $\dfrac{m_1}{m_3}e^{2i\rho}=-\dfrac{1}{s_yc_z^2}\cdot\dfrac{s_x^2c_y^2(c_z^2-s_z^2)-c_xs_ys_z^2(c_xs_y+2s_xc_ys_ze^{i\delta})e^{-2i\delta}}{(s_x^2-c_x^2)s_y-2s_xc_xc_ys_ze^{i\delta}}e^{2i\delta}$ <br><br> $\dfrac{m_2}{m_3}e^{2i\sigma}=+\dfrac{1}{s_yc_z^2}\cdot\dfrac{c_x^2c_y^2(c_z^2-s_z^2)-s_xs_ys_z^2(s_xs_y-2c_xc_ys_ze^{i\delta})e^{-2i\delta}}{(s_x^2-c_x^2)s_y-2s_xc_xc_ys_ze^{i\delta}}e^{2i\delta}$ |
| $E_3:\begin{pmatrix} \mathbf{0} & \times & \times \\ \times & \times & \mathbf{0} \\ \times & \mathbf{0} & \times \end{pmatrix}$ | $\dfrac{m_1}{m_3}e^{2i\rho}=-\dfrac{1}{c_z^2}\cdot\dfrac{s_x^2s_yc_y(c_z^2-s_z^2)+c_xs_z^2[c_xs_yc_y-s_x(s_y^2-c_y^2)s_ze^{i\delta}]e^{-2i\delta}}{(c_x^2-s_x^2)s_yc_y+s_xc_x(c_y^2-s_y^2)s_ze^{i\delta}}e^{2i\delta}$ <br><br> $\dfrac{m_2}{m_3}e^{2i\sigma}=+\dfrac{1}{c_z^2}\cdot\dfrac{c_x^2s_yc_y(c_z^2-s_z^2)+s_xs_z^2[s_xs_yc_y+c_x(s_y^2-c_y^2)s_ze^{i\delta}]e^{-2i\delta}}{(c_x^2-s_x^2)s_yc_y+s_xc_x(c_y^2-s_y^2)s_ze^{i\delta}}e^{2i\delta}$ |
| $F_1:\begin{pmatrix} \times & \mathbf{0} & \mathbf{0} \\ \mathbf{0} & \times & \times \\ \mathbf{0} & \times & \times \end{pmatrix}$ | $\dfrac{m_1}{m_3}e^{2i\rho}=1$ <br><br> $\dfrac{m_2}{m_3}e^{2i\sigma}=1$ |
| $F_2:\begin{pmatrix} \times & \mathbf{0} & \times \\ \mathbf{0} & \times & \mathbf{0} \\ \times & \mathbf{0} & \times \end{pmatrix}$ | $\dfrac{m_1}{m_3}e^{2i\rho}=\dfrac{s_xc_y+c_xs_ys_ze^{-i\delta}}{s_xc_y+c_xs_ys_ze^{+i\delta}}e^{2i\delta}$ <br><br> $\dfrac{m_2}{m_3}e^{2i\sigma}=\dfrac{c_xc_y-s_xs_ys_ze^{-i\delta}}{c_xc_y-s_xs_ys_ze^{+i\delta}}e^{2i\delta}$ |
| $F_3:\begin{pmatrix} \times & \times & \mathbf{0} \\ \times & \times & \mathbf{0} \\ \mathbf{0} & \mathbf{0} & \times \end{pmatrix}$ | $\dfrac{m_1}{m_3}e^{2i\rho}=\dfrac{s_xs_y-c_xc_ys_ze^{-i\delta}}{s_xs_y-c_xc_ys_ze^{+i\delta}}e^{2i\delta}$ <br><br> $\dfrac{m_2}{m_3}e^{2i\sigma}=\dfrac{c_xs_y+s_xc_ys_ze^{-i\delta}}{c_xs_y+s_xc_ys_ze^{+i\delta}}e^{2i\delta}$ |

rameter space of $(\delta,\theta_{\mathrm{chz}})$ and that of $(\theta_x,\theta_y)$ are rather large. Hence pattern C is also favored in phenomenology.

(4) For pattern $D_1$, $\delta$ is restricted to be around $0°$ or $360°$. In particular, the region $90°\leqslant\delta\leqslant270°$ is entirely excluded. $\sin^2 2\theta_{\mathrm{chz}}>0.084$ holds for the allowed range of $\delta$. Different from patterns $A_1$, $B_1$, and C, pattern $D_1$ requires relatively strong correlation between $\theta_x$ and $\theta_y$ (e.g., small values of $\theta_y$ are associated with large values of $\theta_x$ in the allowed parameter space). In this sense, we argue that pattern $D_1$ is less natural in phenomenology, although it has not been ruled out by current experimental data. A similar argument can be made for pattern $D_2$.

It is worth remarking that patterns $D_1$ and $D_2$ were not included into the phenomenologically allowed patterns of $M$ in the previous classification [8,9], where only a very narrow range of $\theta_{\mathrm{atm}}$ around $45°$ (corresponding to maximal or nearly maximal mixing of atmospheric neutrino oscillations [17]) was typically taken. Allowing $\theta_{\mathrm{atm}}$ to vary in a more generous region, as that given in Eq. (10), our present analysis shows that these two patterns are marginally allowed by current data.

## IV. NUMERICAL PREDICTIONS AND FURTHER DISCUSSIONS

A two-zero texture of $M$ has a number of interesting predictions, in particular, for the absolute neutrino masses and the Majorana phases of $CP$ violation [9]. With the help of Eq. (14), one may calculate the mass ratios $m_1/m_3$ and $m_2/m_3$ as well as the Majorana phases $\rho$ and $\sigma$. The absolute neutrino mass $m_3$ can be determined from

$$m_3=\dfrac{1}{\sqrt{\left|1-\left(\dfrac{m_2}{m_3}\right)^2\right|}}\sqrt{\Delta m_{\mathrm{atm}}^2}. \qquad (16)$$
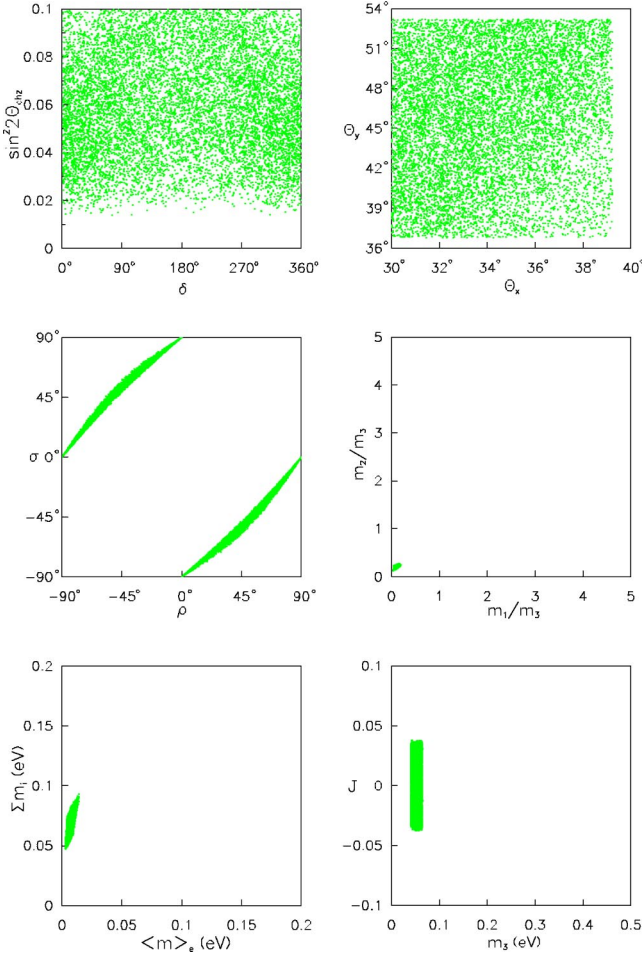
FIG. 1. Pattern $A_1$ of the neutrino mass matrix $M$: allowed regions of $\sin^2 2\theta_{chz}$ vs $\delta$, $\theta_y$ vs $\theta_x$, $\sigma$ vs $\rho$, $m_2/m_3$ vs $m_1/m_3$, $\Sigma m_i$ vs $\langle m \rangle_e$, and $J$ vs $m_3$.



FIG. 2. Pattern $B_1$ of the neutrino mass matrix $M$: allowed regions of $\sin^2 2\theta_{chz}$ vs $\delta$, $\theta_y$ vs $\theta_x$, $\sigma$ vs $\rho$, $m_2/m_3$ vs $m_1/m_3$, $\langle m \rangle_{ee}$ vs $\langle m \rangle_e$, and $J$ vs $m_3$.

Therefore, a full determination of the mass spectrum of three neutrinos is actually possible. Then we may obtain definite predictions for the effective mass of the tritium beta decay,

$$\langle m \rangle_e = m_1 c_x^2 c_z^2 + m_2 s_x^2 c_z^2 + m_3 s_z^2 ; \qquad (17)$$

and that of the neutrinoless double beta decay,

$$\langle m \rangle_{ee} = |m_1 c_x^2 c_z^2 e^{2i\rho} + m_2 s_x^2 c_z^2 e^{2i\sigma} + m_3 s_z^2|. \qquad (18)$$

It is clear that the Dirac phase $\delta$ has no contribution to $\langle m \rangle_{ee}$. Note that $CP$- and $T$-violating asymmetries in normal neutrino oscillations are controlled by $\delta$ or the rephasing-invariant parameter $J = s_x c_x s_y c_y s_z c_z^2 \sin \delta$. Whether $\langle m \rangle_e$ and $\langle m \rangle_{ee}$ can be measured remains an open question. The present experimental upper bounds are $\langle m \rangle_e < 2.2$ eV [18] and $\langle m \rangle_{ee} < 0.35$ eV [19] at the 90% confidence level. The proposed KATRIN experiment is possible to reach the sensitivity $\langle m \rangle_e \sim 0.3$ eV [20], and a number of next-generation experiments for the neutrinoless double beta decay [21] is possible to probe $\langle m \rangle_{ee}$ at the level of 10–50 meV.
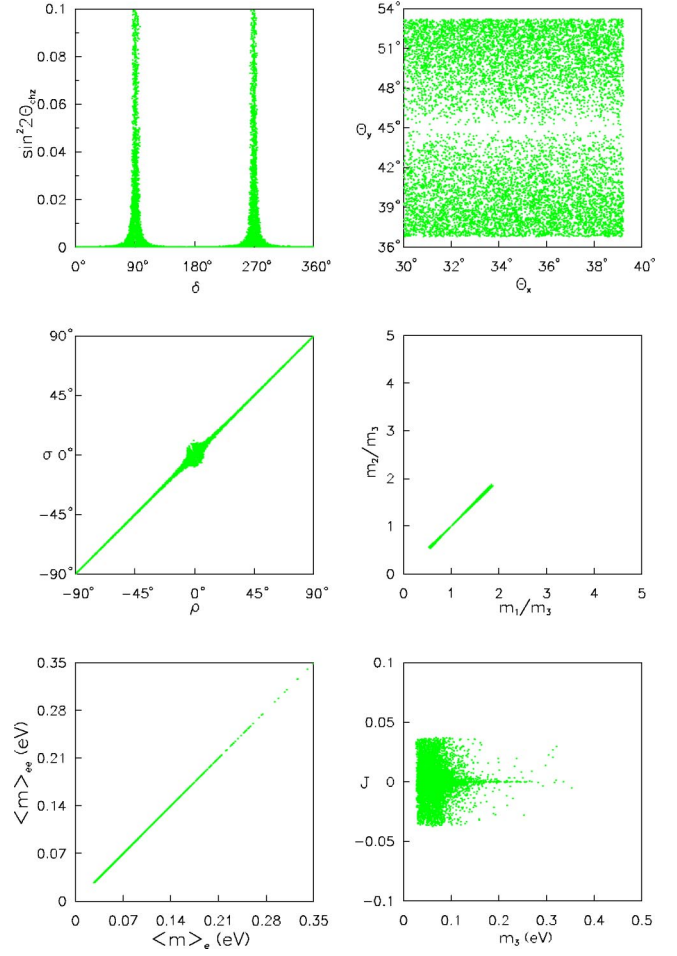
We perform a numerical calculation of $m_2/m_3$ versus $m_1/m_3$, $\sigma$ versus $\rho$, $\langle m \rangle_{ee}$ versus $\langle m \rangle_e$, and $J$ versus $m_3$ for patterns $A_1$, $B_1$, $C$, and $D_1$. The results are shown in Figs. 1–4. Some discussions are in order.

(1) For pattern $A_1$, $\rho \approx \delta/2$ or $\rho \approx \delta/2 - 180°$ and $\sigma \approx \rho \pm 90°$ hold in most cases. Two neutrino mass ratios lie in the ranges $0.033 \leqslant m_1/m_3 \leqslant 0.19$ and $0.13 \leqslant m_2/m_3 \leqslant 0.28$, and the absolute value of $m_3$ is in the range $0.04$ eV $\leqslant m_3 \leqslant 0.065$ eV. As $\langle m \rangle_{ee} = 0$ is a direct consequence of texture $A_1$, we calculate the sum of three neutrino masses $\Sigma m_i$ instead of $\langle m \rangle_{ee}$. The result is $0.047$ eV $\leqslant \Sigma m_i \leqslant 0.093$ eV, in contrast with $0.003$ eV $\leqslant \langle m \rangle_e \leqslant 0.014$ eV. The rephasing invariant of $CP$ violation $J$ is found to lie in the range $-0.037 \leqslant J \leqslant 0.038$. Similar predictions are expected for pattern $A_2$.

(2) For pattern $B_1$, $\rho \approx \sigma \approx \delta - 90°$ or $\rho \approx \sigma \approx \delta - 270°$ holds in most cases. Two neutrino mass ratios $m_1/m_3$ may lie either in the range $0.53 \leqslant m_1/m_3 \leqslant 0.99$ or in the range $1.01 \leqslant m_1/m_3 \leqslant 1.88$, and $m_2/m_3$ may lie either in the range $0.53 \leqslant m_2/m_3 \leqslant 0.99$ or in the range $1.01 \leqslant m_2/m_3 \leqslant 1.88$. The value of $m_3$ is found to be in the range $0.026$ eV $\leqslant m_3 \leqslant 0.35$ eV. Furthermore, we arrive at $0.027$ eV $\leqslant \langle m \rangle_e$
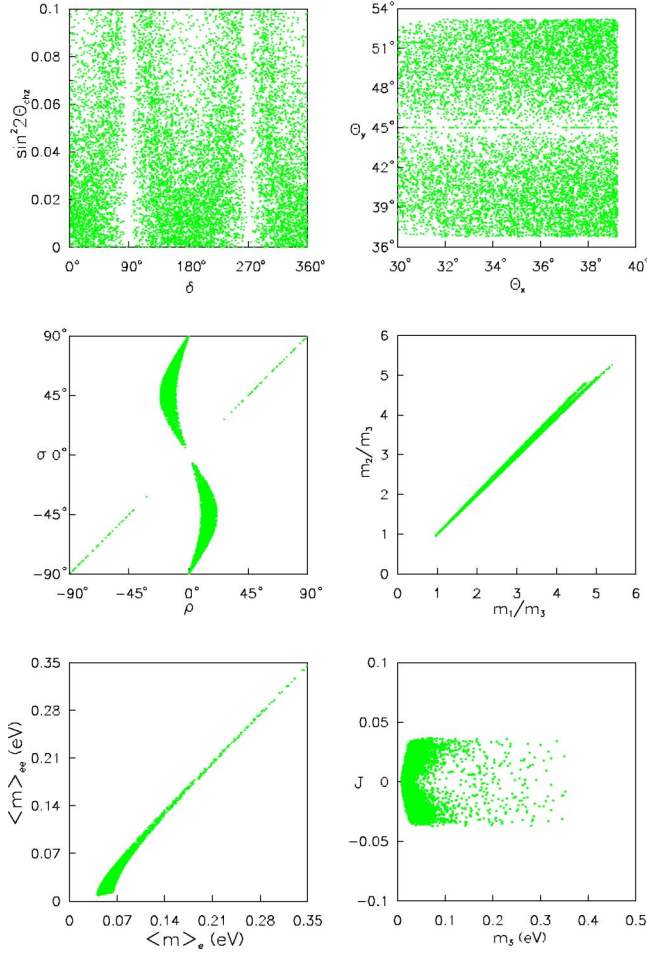
FIG. 3. Pattern C of the neutrino mass matrix $M$: allowed regions of $\sin^2 2\theta_{\text{chz}}$ vs $\delta$, $\theta_y$ vs $\theta_x$, $\sigma$ vs $\rho$, $m_2/m_3$ vs $m_1/m_3$, $\langle m \rangle_{ee}$ vs $\langle m \rangle_e$, and $J$ vs $m_3$.



FIG. 4. Pattern $D_1$ of the neutrino mass matrix $M$: allowed regions of $\sin^2 2\theta_{\text{chz}}$ vs $\delta$, $\theta_y$ vs $\theta_x$, $\sigma$ vs $\rho$, $m_2/m_3$ vs $m_1/m_3$, $\langle m \rangle_{ee}$ vs $\langle m \rangle_e$, and $J$ vs $m_3$.

$\approx \langle m \rangle_{ee} \leq 0.35$ eV as well as $-0.037 \leq J \leq 0.037$. Similar results can be obtained for patterns $B_2$, $B_3$, and $B_4$.

(3) For pattern C, $\sigma \approx \rho$ when $\theta_y$ approaches $45°$; and there is no clear correlation between $\rho$ and $\sigma$ for other values of $\theta_y$. Two neutrino mass ratios $m_1/m_3$ may lie either in the range $0.95 \leq m_1/m_3 \leq 0.99$ or in the range $1.01 \leq m_1/m_3 \leq 5.4$, and $m_2/m_3$ may lie either in the range $0.95 \leq m_2/m_3 \leq 0.99$ or in the range $1.01 \leq m_2/m_3 \leq 5.3$. The value of $m_3$ is found to lie in the range $0.009$ eV $\leq m_3 \leq 0.35$ eV. It is remarkable that $\langle m \rangle_{ee} \approx m_3$ holds to a good degree of accuracy in the allowed space of those input parameters. We also obtain $0.04$ eV $\leq \langle m \rangle_e \leq 0.35$ eV and $-0.037 \leq J \leq 0.037$.

(4) For pattern $D_1$, $\rho \approx \delta - 90°$ or $\rho \approx \delta - 270°$ and $\sigma \approx \rho \pm 90°$ hold. Two neutrino mass ratios lie in the ranges $7.5 \leq m_1/m_3 \leq 8.8$ and $7.35 \leq m_2/m_3 \leq 8.6$, and the absolute value of $m_3$ is in the range $0.005$ eV $\leq m_3 \leq 0.008$ eV. As for the tritium beta decay and neutrinoless double beta decay, we obtain $0.04$ eV $\leq \langle m \rangle_e \leq 0.062$ eV and $0.008$ eV $\leq \langle m \rangle_{ee} \leq 0.014$ eV. The range of $J$ is found to be $-0.014 \leq J \leq 0.011$. Similar predictions can straightforwardly be made for pattern $D_2$.
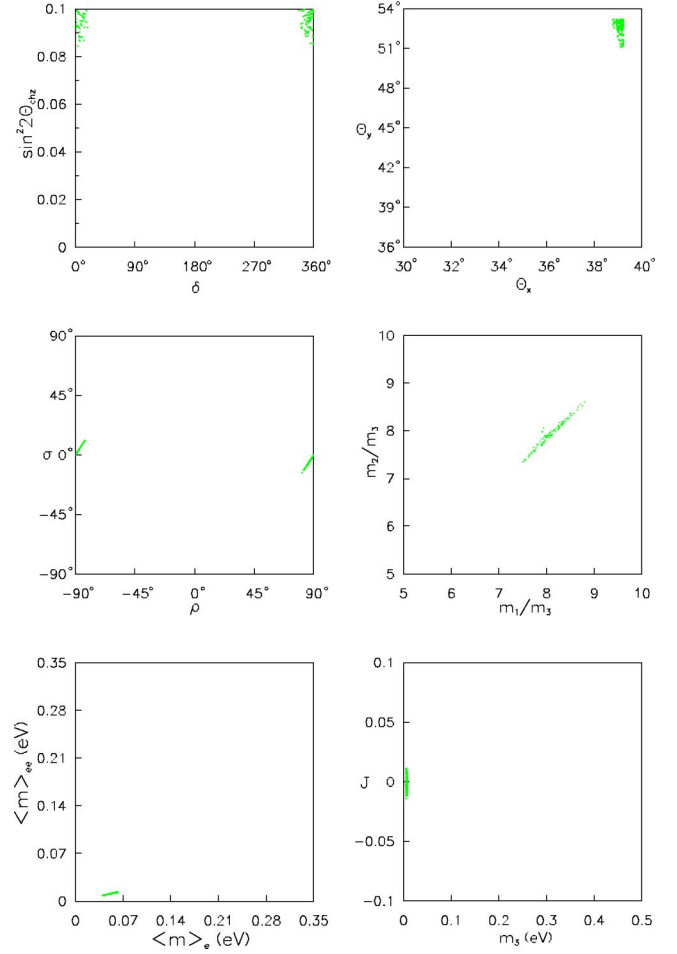
We see that there is no hope to measure both $\langle m \rangle_e$ and $\langle m \rangle_{ee}$, if the neutrino mass matrix $M$ takes pattern $A_1$ or $A_2$. As for categories B and C of $M$, the upper limit of $\langle m \rangle_e$ is close to the sensitivity of the KATRIN experiment ($\sim 0.3$ eV [20]), and that of $\langle m \rangle_{ee}$ is just below the current experimental bound [19].

## V. SUMMARY

In summary, we have discussed some implications of the KamLAND measurment on the lepton flavor mixing matrix $V$ and the neutrino mass matrix $M$. The model-independent constraints on nine elements of $V$ have been obtained up to a reasonable degree of accuracy. Nine two-zero textures of $M$ are found to be compatible with current experimental data, but two of them are only marginally allowed. Instructive consequences of these phenomenologically favored textures of $M$ on the absolute neutrino masses, Majorana phases of $CP$ violation, $\langle m \rangle_e$ and $\langle m \rangle_{ee}$ are numerically explored. Our results will be very useful for model building [22], in order to understand why neutrino masses are so tiny and why two of the lepton flavor mixing angles are so large.

Finally, it is worth remarking that a specific texture of lepton mass matrices may not be preserved to all orders or at any energy scales in the unspecified interactions from which lepton masses are generated. Nevertheless, those phenomenologically favored textures at low energy scales, no matter whether they are of the two-zero form or other forms, are possible to provide enlightening hints at the underlying dynamics of lepton mass generation at high energy scales.

[1] KamLAND Collaboration, K. Eguchi *et al.*, Phys. Rev. Lett. **90**, 021802 (2003).

[2] L. Wolfenstein, Phys. Rev. D **17**, 2369 (1978); S.P. Mikheyev and A.Yu. Smirnov, Sov. J. Nucl. Phys. **42**, 913 (1985).

[3] K2K Collaboration, M.H. Ahn *et al.*, Phys. Rev. Lett. **90**, 041801 (2003).

[4] SNO Collaboration, Q.R. Ahmad *et al.*, Phys. Rev. Lett. **89**, 011301 (2002); **89**, 011302 (2002).

[5] For a review, see C.K. Jung, C. McGrew, T. Kajita, and T. Mann, Annu. Rev. Nucl. Part. Sci. **51**, 451 (2001).

[6] CHOOZ Collaboration, M. Apollonio *et al.*, Phys. Lett. B **420**, 397 (1998); Palo Verde Collaboration, F. Boehm *et al.*, Phys. Rev. Lett. **84**, 3764 (2000).

[7] Z.Z. Xing, Phys. Rev. D **65**, 077302 (2002); **65**, 113010 (2002).

[8] P.H. Frampton, S.L. Glashow, and D. Marfatia, Phys. Lett. B **536**, 79 (2002).

[9] Z.Z. Xing, Phys. Lett. B **530**, 159 (2002); **539**, 85 (2002).

[10] C. Jarlskog, Phys. Rev. Lett. **55**, 1039 (1985).

[11] M. Fukugita and M. Tanimoto, Phys. Lett. B **515**, 30 (2001).

[12] H. Fritzsch and Z.Z. Xing, Phys. Lett. B **517**, 363 (2001); Phys. Rev. D **57**, 594 (1998).

[13] G.L. Fogli *et al.*, hep-ph/0212127.

[14] V. Barger and D. Marfatia, hep-ph/0212126; P. Creminelli, G. Signorelli, and A. Strumia, J. High Energy Phys. **05**, 052 (2001); M. Maltoni, T. Schwetz, and J.W.F. Valle, hep-ph/0212129.

[15] Super-Kamiokande Collaboration, M. Shiozawa, talk given at Neutrino 2002, Munich, 2002.

[16] W.L. Guo and Z.Z. Xing, hep-ph/0211315.

[17] See, e.g., H. Fritzsch and Z.Z. Xing, Phys. Lett. B **372**, 265 (1996); **440**, 313 (1998); Phys. Rev. D **61**, 073016 (2000).

[18] Particle Data Group, K. Hagiwara *et al.*, Phys. Rev. D **66**, 010001 (2002).

[19] Heidelberg-Moscow Collaboration, H.V. Klapdor-Kleingrothaus, hep-ph/0103074, and references therein.

[20] V. Aseev *et al.*, talks given at the International Workshop on Neutrino Masses in the Sub-eV Ranges, Bad Liebenzell, Germany, 2001; homepage: http://www-ikl.fzk.de/tritium

[21] S.M. Bilenky, C. Giunti, J.A. Grifols, and E. Massó, hep-ph/0211462, and references therein.

[22] For recent reviews with extensive references, see H. Fritzsch and Z.Z. Xing, Prog. Part. Nucl. Phys. **45**, 1 (2000); G. Altarelli and F. Feruglio, in *Neutrino Mass*, Springer Tracts in Modern Physics, edited by G. Altarelli and K. Winter (Springer-Verlag, Berlin, in press), hep-ph/0206077.